

A numerical investigation of phase change effects in porous materials

K. VAFAI and H. C. TIEN

Department of Mechanical Engineering, The Ohio State University, Columbus, OH 43210, U.S.A.

(Received 1 September 1988 and in final form 5 December 1988)

Abstract—In this paper, a numerical study of heat and mass transfer with phase change in porous materials is performed. The problem is modelled by a system of transient inter-coupled equations governing the two-dimensional multiphase transport process in porous media. The solution algorithm allows full simulation without any significant simplifications. The variations and the interrelationship between the temperature, vapor density, condensation rate, liquid content and the fluid velocity fields are demonstrated and discussed in detail. It is found that the aspect ratio of the porous matrix does not have a significant effect on the Nusselt number results. Furthermore, it is found that the one-dimensional model is not valid when the boundaries of the porous matrix are subjected to a small or zero pressure difference and that the constant pressure simplification would generate significant errors under some circumstances. The present analysis, which presents a full simulation of the problem for the first time, can be applied to a class of problems on heat and mass transport with phase change through a porous medium.

1. INTRODUCTION

A NUMBER of applications in thermal engineering require a good working knowledge of heat and mass transfer in porous media. Such applications include building insulations, heat exchangers, grain storage, energy conservation, drying technology, oil extraction and geothermal systems, etc. An important topic in the area of energy conservation and building insulation design relates to the influence of condensation on the thermal performance of a porous insulation matrix. Water vapor condensation can take place anywhere in a porous insulation when the vapor density is greater than the saturation vapor density which corresponds to the local temperature at that point. The condensation phenomenon has been observed in a porous wall insulation especially when the insulating material is exposed to large temperature differences and high humidity environments. As the condensation occurs, the latent heat of vaporization is released acting as a heat source in the heat transfer process. Furthermore, the liquid phase resulting from condensation will cause a significant increase in the energy transfer across the insulation and hence it affects the thermal performance of the insulation. In addition, the condensate deteriorates the quality of the porous materials.

In general, a wet porous insulation consists of three phases which are the solid matrix, the liquid water, and a binary gas phase composed of air and water vapor. In the gas phase, there is vapor diffusion due to the vapor concentration gradients, bulk convection due to the density variation induced by temperature gradients, and air infiltration due to the small difference in gas pressure across the insulation. There is

heat conduction in all three phases, heat convection in the gas phase and the liquid phase if the liquid phase is mobile. In addition, there is heat transfer caused by phase change at the gas-liquid interface.

There has been some experimental work on this subject [1-3]. However, these studies were conducted for some specific applications and hence the findings can only be applied to some particular problems. In the semi-analytical work of ref. [4], the condensation process is characterized in terms of three distinct regimes. However, analytical solutions [4] based on one-dimensional formulation were obtained for the second regime (quasi-steady approach) only. In a previously related work [5], the condensation problem was modelled as one-dimensional multiphase heat and mass transport accompanied by phase change. The transient as well as the steady-state solutions were obtained. In another previous work [6] the two-dimensional unsteady transport process was considered, however, several important simplifying assumptions were made in arriving at the solutions. Apparently there is indeed a need for a more rigorous and extensive investigation of this subject without any significant simplifications.

This paper investigates transient two-dimensional heat and mass transport accounting for phase change in a porous matrix. Different versions of numerical schemes are thoroughly studied in order to examine the stability and accuracy. The variations and the inter-coupling effects of the important field variables such as temperature, vapor density, condensation rate and liquid content are presented. The transient heat transfer rate through the insulation is quantified and the validity of using a one-dimensional or constant pressure assumption is investigated. The location and

NOMENCLATURE

A	aspect ratio, \bar{H}/\bar{L}	\bar{R}_v	vapor gas constant [$\text{N m kg}^{-1} \text{K}^{-1}$]
B	Biot number referring to heat transfer, $\bar{h}\bar{L}/\bar{k}_{\text{eff},0}$	s	scaled fractional liquid saturation, $(s_\beta - s_{\beta p})/(1 - s_{\beta p})$
B^*	Biot number referring to mass transfer, $\bar{h}^*\bar{L}/\bar{\alpha}_{\text{eff},0}$	s_β	fractional liquid saturation, $\varepsilon_\beta/(\varepsilon_\beta + \varepsilon_v)$
B_v	Biot number referring to species transport, $\bar{h}_v\bar{L}/\bar{\alpha}_{\text{eff},0}$	$s_{\beta p}$	saturation for the immobile liquid
\bar{c}_i	dimensional heat capacity for the i th phase at constant pressure [$\text{W s kg}^{-1} \text{K}^{-1}$]	t	dimensionless time, $\bar{t}/(\bar{L}^2/\bar{\alpha}_{\text{eff},0})$
\bar{c}_0	reference heat capacity [$\text{W s kg}^{-1} \text{K}^{-1}$]	T	dimensionless temperature, $\bar{T}/\Delta\bar{T}$
\bar{C}_p	average heat capacity [$\text{W s kg}^{-1} \text{K}^{-1}$]	\bar{T}_h	reference temperature for the hot side of the insulation [K]
$\bar{D}_{v,\text{eff}}$	effective vapor diffusivity coefficient [$\text{m}^2 \text{s}^{-1}$]	\bar{T}_c	reference temperature for the cold side of the insulation [K].
\mathbf{g}	dimensionless gravity vector	Greek symbols	
\bar{h}	heat transfer coefficient [$\text{W m}^{-2} \text{K}^{-1}$]	$\bar{\alpha}_{\text{eff},0}$	reference effective thermal diffusivity, $\bar{k}_{\text{eff},0}/(\bar{\rho}_0\bar{c}_0)$ [$\text{m}^2 \text{s}^{-1}$]
\bar{h}^*	mass transfer coefficient [m s^{-1}]	ε	volume fraction
\bar{h}_v	species transfer coefficient [m s^{-1}]	$\bar{\mu}_\beta$	liquid dynamic viscosity [$\text{kg m}^{-1} \text{s}^{-1}$]
$\Delta\bar{h}_{\text{vap}}$	enthalpy of vaporization per unit mass [J kg^{-1}]	$\bar{\mu}_\gamma$	gas dynamic viscosity [$\text{kg m}^{-1} \text{s}^{-1}$]
\bar{H}	height of the porous insulation [m]	$\bar{\rho}$	dimensional total density defined in equation (16) [kg m^{-3}]
\bar{k}_i	dimensional thermal conductivity for phase i [$\text{W m}^{-1} \text{K}^{-1}$]	ρ_i	dimensionless density for phase i , $\bar{\rho}_i/\bar{\rho}_{i,0}$
$\bar{k}_{c,T}$	$-\partial\langle\bar{p}_c\rangle/\partial\langle\bar{T}\rangle$ [$\text{N m}^{-2} \text{K}^{-1}$]	ρ_v	dimensionless vapor density, $\bar{\rho}_v/\bar{\rho}_{v,0}$
\bar{k}_c	$-\partial\langle\bar{p}_c\rangle/\partial\varepsilon_\beta$ [N m^{-2}]	$\bar{\sigma}_{\beta\gamma}$	surface tension at the gas and liquid interface [N m^{-1}]
\bar{k}_{eff}	dimensional effective thermal conductivity [$\text{W m}^{-1} \text{K}^{-1}$]	ω	relative humidity.
\bar{K}	permeability [m^2]	Subscripts	
\bar{K}_β	effective liquid permeability [m^2]	a	air phase
\bar{K}_γ	effective gas permeability [m^2]	eff	effective properties
$K_{r,\beta}$	relative permeability for the liquid phase	i	i th phase
$K_{r,\gamma}$	relative permeability for the gas phase	s	saturation quantities
\bar{L}	thickness of the insulation [m]	v	vapor phase
Le	Lewis number, $\bar{\alpha}_{\text{eff},0}/\bar{D}_{v,\text{eff}}$	x	component in the x -direction
\bar{m}	dimensional condensation rate [$\text{kg m}^{-3} \text{s}^{-1}$]	β	liquid phase
p_a	dimensionless air pressure, $p_a/\bar{p}_{a,0}$	γ	gas phase
\bar{p}_c	capillary pressure, $\bar{p}_v - \bar{p}_\beta$ [N m^{-2}]	σ	solid matrix
p_v	dimensionless vapor pressure, $\bar{p}_v/\bar{p}_{v,0}$	0	reference quantities
p_γ	dimensionless gas phase pressure, $\bar{p}_\gamma/\bar{p}_{\gamma,0}$	∞	ambient quantities in the surroundings.
Pe	Peclet number, $\bar{v}_{\gamma,0}\bar{L}/\bar{\alpha}_{\text{eff},0}$	Superscript	
\bar{r}	characteristic length of the porous matrix [m]	-	dimensional quantities.
\bar{R}_a	air gas constant [$\text{N m kg}^{-1} \text{K}^{-1}$]	Other symbol	
		$\langle \rangle$	'local volume average' of the quantity.

regions of high liquid accumulation are analyzed. Also, the interesting effects of variations of the aspect ratios and humidity levels on the condensation rate, liquid accumulation and the energy transfer are also discussed in detail.

2. ANALYSIS

The governing equations for the multiphase transport process in a porous medium are derived by using

the local volume averaging technique. An averaging volume V which is bounded by a closed surface in the porous medium is composed of three phases, the solid phase V_s , the liquid phase $V_\beta(t)$, and the gas phase $V_\gamma(t)$. The spatial average for a quantity Ψ is defined as

$$\langle \Psi \rangle = \frac{1}{V} \int_V \Psi \, dV. \quad (1)$$

Another important averaging quantity of interest is

the intrinsic phase average which is given by

$$\langle \Psi_\alpha \rangle^\alpha = \frac{1}{V_\alpha(t)} \int_{V_\alpha(t)} \Psi_\alpha dV \quad (2)$$

where Ψ_α is a quantity associated with phase α .

The derivation of the governing equations for heat and mass transport in a porous insulation is based on Whitaker's work [7] which involves a significant amount of mathematical manipulation. The only major assumptions which are made in order to arrive at the governing equations are: (1) the porous insulation material is homogeneous and isotropic; and (2) the porous system which consists of the solid, liquid, and gas phases is assumed to be in local thermodynamic equilibrium. Aside from these assumptions, the governing equations are very general and the results which are presented and discussed in this paper can be applied to a class of problems in heat and mass transfer in porous media with phase change. The governing equations after nondimensionalization are given as follows:

thermal energy equation

$$\begin{aligned} \frac{\partial \langle T \rangle}{\partial t} + \frac{P_1 P_2 P_{18}}{P_{19}} \psi_\epsilon \langle \mathbf{v}_\beta \rangle \cdot \nabla \langle T \rangle \\ + \frac{P_3 P_4 P_{18} Pe}{P_{19}} \langle \rho_\gamma \rangle' \langle \mathbf{v}_\gamma \rangle \cdot \nabla \langle T \rangle \\ + \frac{P_{18}}{P_{19}} \langle \dot{m} \rangle = P_{18} \nabla^2 \langle T \rangle + \frac{P_{18}}{P_{19}} \nabla P_{19} \cdot \nabla \langle T \rangle; \end{aligned} \quad (3)$$

liquid phase equation of motion

$$\langle \mathbf{v}_\beta \rangle = -K_{r\beta} (\nabla \epsilon_\beta + \psi_T \nabla \langle T \rangle - \psi_g \mathbf{g}); \quad (4)$$

liquid phase continuity equation

$$\frac{\partial \epsilon_\beta}{\partial t} + \psi_c \nabla \cdot \langle \mathbf{v}_\beta \rangle + \frac{1}{P_1 P_6} \langle \dot{m} \rangle = 0; \quad (5)$$

gas phase equation of motion

$$\langle \mathbf{v}_\gamma \rangle = P_{20} K_{r\gamma} (-\nabla \langle p_\gamma \rangle' + P_5 \langle \rho_\gamma \rangle' \mathbf{g}); \quad (6)$$

gas phase continuity equation

$$\frac{\partial}{\partial t} (\epsilon_\gamma \langle \rho_\gamma \rangle') + Pe \nabla \cdot (\langle \rho_\gamma \rangle' \langle \mathbf{v}_\gamma \rangle) - \frac{1}{P_4 P_6} \langle \dot{m} \rangle = 0; \quad (7)$$

gas phase diffusion equation

$$\begin{aligned} \frac{\partial}{\partial t} (\epsilon_\gamma \langle \rho_v \rangle') + Pe \nabla \cdot (\langle \rho_v \rangle' \langle \mathbf{v}_\gamma \rangle) - \frac{1}{P_4 P_6 P_{11}} \langle \dot{m} \rangle \\ = \frac{1}{Le} \nabla \cdot \left[\langle \rho_\gamma \rangle' \nabla \left(\frac{\langle \rho_v \rangle'}{\langle \rho_\gamma \rangle'} \right) \right]; \end{aligned} \quad (8)$$

volume constraint

$$\epsilon_\sigma + \epsilon_\beta + \epsilon_\gamma = 1; \quad (9)$$

thermodynamic relations

$$\langle p_v \rangle' = P_9 \langle \rho_v \rangle' \langle T \rangle \quad (10)$$

$$\langle p_a \rangle' = P_9 \langle \rho_a \rangle' \langle T \rangle \quad (11)$$

$$\langle \rho_\gamma \rangle' = P_{11} \langle \rho_v \rangle' + P_{12} \langle \rho_a \rangle' \quad (12)$$

$$\langle p_\gamma \rangle' = P_{13} \langle p_v \rangle' + P_{14} \langle p_a \rangle' \quad (13)$$

$$\langle \rho_{v,s} \rangle' = \frac{1}{P_9 \langle T \rangle} \exp \left(-\frac{P_{15} + P_{16}}{\langle T \rangle} + \frac{P_{16}}{\langle T_0 \rangle} \right) \quad (14)$$

where the dimensionless variables and the controlling parameters are defined in the Appendix. The variable properties in the porous insulation are

$$\bar{K}_{eff} \cong \epsilon_\sigma \bar{K}_\sigma + \epsilon_\beta \bar{K}_\beta + \epsilon_\gamma \frac{(\bar{K}_v \langle \bar{\rho}_v \rangle' + \bar{K}_a \langle \bar{\rho}_a \rangle')}{(\langle \bar{\rho}_v \rangle' + \langle \bar{\rho}_a \rangle')} \quad (15)$$

$$\bar{\rho} = \epsilon_\sigma \bar{\rho}_\sigma + \epsilon_\beta \bar{\rho}_\beta + \epsilon_\gamma (\langle \bar{\rho}_v \rangle' + \langle \bar{\rho}_a \rangle') \quad (16)$$

$$\bar{C}_p = \frac{\epsilon_\sigma \bar{\rho}_\sigma \bar{c}_\sigma + \epsilon_\beta \bar{\rho}_\beta \bar{c}_\beta + \epsilon_\gamma (\langle \bar{\rho}_v \rangle' \bar{c}_v + \langle \bar{\rho}_a \rangle' \bar{c}_a)}{\bar{\rho}} \quad (17)$$

$$\bar{\alpha}_{eff} = \frac{\bar{K}_{eff}}{\bar{\rho} \bar{C}_p} \quad (18)$$

The main variables of interest in the above equations are the temperature T , the liquid volume fraction ϵ_β , the vapor density ρ_v , the gas density ρ_γ , the gas volume fraction ϵ_γ , and the condensation rate \dot{m} . The quantities with a subscript '0' denote the reference quantities, and the variables with a bar on top of them refer to dimensional quantities. The controlling parameters P_1, P_2, P_4, P_6, P_9 , and $P_{11}-P_{14}$, which are defined in the Appendix, are constants and are fixed by the choice of the reference quantities. P_3, P_{18} and P_{19} are the parameters which vary with the variation of the properties. P_{15} and P_{16} are the non-dimensional parameters which appear in the Clausius-Clapeyron equation. P_{15} accounts for the Kelvin effect and is far less dominant than P_{16} in determining the saturation vapor density. P_5, Pe and P_{20} have a direct influence on the gas phase convective terms. P_5 accounts for the body force, and Pe and P_{20} affect the numerical stability. ψ_g and ψ_T describe the relative importance of gravity and thermal gradients in transporting the liquid phase. Finally Le and ψ_ϵ are the controlling parameters which characterize the importance of the vapor diffusion and liquid transport relative to the energy transport.

It should be noted that non-Darcian effects are assumed to be negligible in this study. This assumption is justified due to the following reasons. Vasseur *et al.* [8] used the results of ref. [9] to examine the validity of Darcy's law. Two conditions which respectively characterize the inertia and the boundary effects, should be satisfied if the results obtained from Darcy's law are to be within a 10% error band

$$\bar{U} < \frac{6 \times 10^{-3} \bar{v}}{(1 - \epsilon_\sigma) F \sqrt{\bar{K}}} \quad \text{and} \quad \bar{L} > Pr \sqrt{(\bar{K}/(1 - \epsilon_\sigma))} \quad (19)$$

where \bar{U} is the characteristic fluid velocity, \bar{v} the kinematic viscosity, $(1 - \epsilon_\sigma)$ the porosity, F a coefficient related to the inertia parameter, \bar{K} the permeability, \bar{L} the characteristic length of the porous material, and

Pr is the Prandtl number. Based on the data used in the calculation, these two conditions are apparently satisfied. The dispersion effects are also neglected in this study. It is also noted that the effective gas permeability \bar{K}_γ and the effective liquid permeability for partially liquid saturated media \bar{K}_β can be expressed as the multiplication of the permeability \bar{K} and the relative permeabilities, $K_{r\beta}$ and $K_{r\gamma}$, as

$$\begin{aligned} \bar{K}_\gamma &= K_{r\gamma} \bar{K} \\ \bar{K}_\beta &= K_{r\beta} \bar{K}. \end{aligned} \tag{20}$$

Based on the relative permeability model suggested by Wyllie [10] which agrees well with the data in Fatt and Klikoff [11] and is also used in Udell [12], the relative permeabilities are taken to have the following forms:

$$\begin{aligned} K_{r\beta} &= s^3 \\ K_{r\gamma} &= (1-s)^3 \end{aligned} \tag{21}$$

where

$$s = \frac{s_\beta - s_{\beta p}}{1 - s_{\beta p}} \tag{22}$$

and

$$s_\beta = \frac{\epsilon_\beta}{\epsilon_\beta + \epsilon_\gamma}. \tag{23}$$

The variable $s_{\beta p}$ is the saturation of the liquid in the pendular state in the porous medium. Below this saturation, the liquid is essentially immobile due to no inter-pore connections. There were no concrete experimental data available for $s_{\beta p}$, however a value of 0.1 was found to be a reasonable one. This value was also used in Kaviany and Mittal's work on drying [13].

2.1. Convective boundary conditions

In addition to the specified-value type of boundary conditions, another type of boundary conditions is also frequently encountered. The convective boundary conditions at the porous media-surrounding gas interface were obtained in a way which was similar to the derivation of the governing equations [14]. The non-dimensional boundary conditions for the mass, energy and species balance are written as follows:

mass balance

$$\begin{aligned} (P_1 \psi_\epsilon \langle v_\beta \rangle + Pe P_4 \langle \rho_\gamma \rangle' \langle v_\gamma \rangle) \cdot \mathbf{n} \\ = B^* P_4 (\langle \rho_\gamma \rangle' - \rho_x); \end{aligned} \tag{24}$$

energy balance

$$P_1 P_6 \psi_\epsilon \langle v_\beta \rangle \cdot \mathbf{n} + P_{19} \nabla T \cdot \mathbf{n} = B(T_\infty - \langle T \rangle); \tag{25}$$

species balance

$$\begin{aligned} \left[P_1 \psi_\epsilon \langle v_\beta \rangle + Pe P_4 P_{11} \langle \rho_\gamma \rangle' \langle v_\gamma \rangle \right. \\ \left. - \frac{P_4 P_{11}}{Le} \langle \rho_\gamma \rangle' \nabla \left(\frac{\langle \rho_\gamma \rangle'}{\langle \rho_\gamma \rangle'} \right) \right] \cdot \mathbf{n} \\ = B_v P_4 P_{11} (\langle \rho_\gamma \rangle' - \rho_{v,\infty}) \end{aligned} \tag{26}$$

where \mathbf{n} is the unit normal vector which points out from the porous medium into the surrounding gas phase, and B^* , B and B_v are the Biot numbers referring to, the mass transfer, heat transfer, and species transport, respectively. In particular for the impermeable and insulated boundary conditions, all of these three Biot numbers are equal to zero, and hence the right-hand sides of equations (24)–(26) reduce to zero.

3. PROBLEM STATEMENT

To investigate two-dimensional transient heat and moisture transport accounting for phase change in a porous insulation, a systematic study has been performed on a case which is important from a fundamental point of view as well as the application side. The schematic diagram is shown in Fig. 1. The top and bottom boundaries are insulated and impermeable, while the left and right boundaries are exposed to two different environments, a hot and humid environment on the left-hand side and a cooler environment on the right-hand side. The boundary conditions on the temperature, relative humidity, liquid content and the gas phase pressure for the left and right boundaries are specified as

$$\begin{aligned} T_h &= T(x = 0, y, t) = 15.4 \\ T_c &= T(x = 1, y, t) = 14.65 \end{aligned} \tag{27}$$

$$\begin{aligned} 0 < \omega_h &= \omega(x = 0, y, t) \leq 1 \\ \omega_c &= \omega(x = 1, y, t) = 1 \end{aligned} \tag{28}$$

$$\begin{aligned} \epsilon_\beta(x = 0, y, t) &= 5.0 \times 10^{-5} \\ \epsilon_\beta(x = 1, y, t) &= 0 \end{aligned} \tag{29}$$

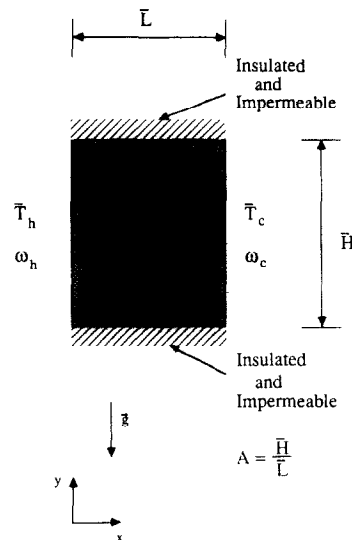


FIG. 1. Schematic diagram of a two-dimensional porous matrix.

$$\begin{aligned}
 p_\gamma(x = 0, y, t) &= 1 \\
 p_\gamma(x = 1, y, t) &= 1.
 \end{aligned}
 \tag{30}$$

It should be noted that the above non-dimensional temperatures translate into $\bar{T}_h = 308$ K and $\bar{T}_c = 293$ K which are based on physical grounds. For the top and bottom walls, equations (24)–(26) were employed. Since the top and bottom boundaries are subjected to insulated and impermeable boundary conditions, the Biot numbers, B^* , B and B_v , are set equal to zero in equations (24)–(26).

3.1. Initial conditions

$$\begin{aligned}
 T(x, y, t = 0) &= 14.65 \\
 \omega(x, y, t = 0) &= 1 \\
 \varepsilon_\beta(x, y, t = 0) &= 0 \\
 p_\gamma(x, y, t = 0) &= 1.
 \end{aligned}
 \tag{31}$$

To evaluate the heat transfer across the porous insulation matrix, the non-dimensional heat transfer rate at the hot surface, Nu_h , which includes both the heat as well as the mass transfer is given as

$$Nu_h = \frac{\int_0^A \left(-P_{19} \frac{\partial T}{\partial x} + P_3 P_4 P_e \rho_\gamma v_{\gamma x} T + P_1 P_2 \psi_\beta v_{\beta x} T \right) \Big|_{x=0} dy}{AP_{19}(T_h - T_c)}.
 \tag{32}$$

The Nusselt number, as defined in equation (32), accounts for the contribution of heat conduction, infiltration and bulk convection. The physical data used in the numerical experiments, which were based on the use of a fibrous insulation, are listed in Table 1. It should be noted that even though the Kelvin effect has been taken into account in equation (14), a surface tension of 0.07 kg m⁻² translates into $P_{15} \ll P_{16}$ if $O(\bar{r}) > 10^{-9}$ m. This fact was also given in ref. [15] where it was mentioned that surface tension presented very little effect on the saturation vapor pressure.

4. SOLUTION METHODOLOGY

At first, it seemed that the governing equations were well suited to be solved by the MacCormack method

Table 1. Physical data

(a) Reference quantities

$\bar{\rho}_0$ (kg m ⁻³)	\bar{c}_0 (J kg ⁻¹ K ⁻¹)	$\bar{\rho}_{v,0}$ (kg m ⁻³)	$\bar{\rho}_{a,0}$ (kg m ⁻³)	$\bar{\rho}_{\gamma,0}$ (kg m ⁻³)	\bar{T}_0 (K)	$\bar{p}_{\gamma,0}$ (N m ⁻²)	$\bar{K}_{eff,0}$ (W m ⁻¹ K ⁻¹)
76.89	842	0.03966	1.08216	1.12182	308	1.013×10^5	0.026

(b) Solid phase

ε_σ	\bar{L} (m)	$\bar{\rho}_\sigma$ (kg m ⁻³)	\bar{c}_σ (J kg ⁻¹ K ⁻¹)	\bar{K}_σ (W m ⁻¹ K ⁻¹)
0.03	0.12	2563	835	0.043

(c) Liquid phase

$\bar{\rho}_\beta$ (kg m ⁻³)	\bar{c}_β (J kg ⁻¹ K ⁻¹)	\bar{K}_β (W m ⁻¹ K ⁻¹)	$\bar{\mu}_\beta$ (kg m ⁻¹ s ⁻¹)
1000	4182	0.603	0.8×10^{-3}

(d) Gas phase

\bar{c}_v (J kg ⁻¹ K ⁻¹)	\bar{c}_a (J kg ⁻¹ K ⁻¹)	\bar{K}_v (W m ⁻¹ K ⁻¹)	\bar{K}_a (W m ⁻¹ K ⁻¹)	\bar{R}_v (J kg ⁻¹ K ⁻¹)	\bar{R}_a (J kg ⁻¹ K ⁻¹)	$\bar{\mu}_\gamma$ (kg m ⁻¹ s ⁻¹)
1866	1000	0.0191	0.0262	462	287	1.846×10^{-5}

(e) Other quantities

\bar{K} (m ²)	$\bar{D}_{v,eff}$ (m ² s ⁻¹)	ΔT (K)	$\Delta \bar{h}_{vap}$ (J kg ⁻¹)	$\bar{\sigma}_{\beta\gamma}$ (kg s ⁻²)
7.25×10^{-10}	2.8×10^{-5}	20	2.4425×10^6	0.07

(either explicit or implicit) or the Beam-Warming method, which are used to solve Navier-Stokes equations [16]. However, the difficulty in employing such numerical schemes to solve these governing equations is twofold. First, these transport equations are so complicated that they cannot be rearranged into conservative form without a loss of accuracy, as both the MacCormack and the Beam-Warming methods can be used only when the equations are cast in the conservative form. Furthermore, the source terms in some of the governing equations add on an additional difficulty when we applied such schemes to solve the governing equations. These problems were also encountered by Reddy *et al.* [17]. Based on the above reasons, an explicit finite difference method was used in order to obtain the most accurate results. This numerical scheme consists of two different formats in time and space depending on whether the phase change occurs or not. According to the experimental results of Langlais *et al.* [3], those values of $\varepsilon_\beta < 10^{-5}$ are considered to be part of the adsorbed water. Therefore, the condensation rate is set equal to zero at any time and location where $\varepsilon_\beta < 10^{-5}$. When $\varepsilon_\beta < 10^{-5}$, vapor cannot be regarded as being at the saturation state any more and hence no bulk condensation is possible. The detailed description of this two-phase algorithm is given in Vafai and Whitaker's work [6].

In the forementioned numerical scheme, the spatial derivatives are discretized by the central differencing except for most of the convective terms which are approximated by several different forms of upwind differencing. Since the physical phenomenon for this problem is highly transient and complicated, the required time step size must be quite small. Numerical experimentation was conducted for different versions of upwind differencing methods such as first-order upwind, third-order upwind, and third-order upwind plus fourth-order artificial viscosity, etc., to determine the accuracy and numerical stability of each scheme. After extensive numerical experimentation was performed on all of these different forms of the upwind differencing, the first-order upwind difference scheme was chosen to approximate the convective terms, except in the gas continuity equation, due to its numerical stability. This numerical scheme was further compared with several semi-implicit schemes (i.e. the implicit schemes were used in solving some of the transport equations which have strong convective terms). It was found that the total computational time could not be reduced by using the semi-implicit schemes. As a side product of these extensive comparisons it was found that the results from all of the above-mentioned schemes (explicit or semi-implicit) were in very good agreement with each other.

It was found that the higher the gas permeability is, the stronger the convection terms will be, and hence a smaller time step size is required. This is because the gas phase permeability directly affects the advection terms and hence it has a very significant effect in

determining the time step size. This fact can be easily seen after examining the expression for P_{20} in the Appendix. For this reason, the value of permeability used in this work was chosen to represent a typically high porosity insulation material so that, in addition to corresponding to a very important application, it will also highlight some of the pertinent features of the analysis. For such a highly porous material, the required time step size is relatively small. Of course the time step size is also affected by the number of grids. The required time step size becomes much smaller as we refine the grids.

5. RESULTS AND DISCUSSION

As mentioned earlier, this work is aimed at a fundamental investigation of the thermal behavior of the porous material and the dynamic response and the interaction between the field variables such as temperature, liquid content, vapor density, and the condensation rate in a two-dimensional porous medium. It is also aimed at investigating the effects of the aspect ratios, humidity levels and some other pertinent physical parameters.

Figure 2 shows the temperature distribution inside a porous matrix at four different times. As shown in Fig. 2 the interior temperature of the insulation material is found to increase with time when the temperature is suddenly increased at the left boundary. The temperature rise results from simultaneous heat conduction and heat convection along with condensation which acts as a local heat source. The increase in temperature starts from the region which is close to the external boundary which is at a higher temperature and then gradually moves inwards into the porous matrix. This *wave-like* propagation was also observed for the vapor density, liquid content and condensation rate as it can be seen in Figs. 3–5. For brevity, the contours for the gas phase density are not presented here. However, the same type of *wave-like* propagation was observed for $\langle \rho_v \rangle$. It should be mentioned that in all of the three-dimensional plots for the condensation rate, a positive $\langle \dot{m} \rangle$ corresponds to condensation whereas a negative $\langle \dot{m} \rangle$ corresponds to evaporation. The times t_1 , t_2 , t_3 and t_4 in Figs. 2–5 were chosen so as to demonstrate the significant regimes and variations of the field variables. A very important result which becomes apparent from this investigation is that the common assumption of setting $\langle \rho_v \rangle = \text{const.}$ is not valid at all. This of course, is to be expected as this assumption does not satisfy the continuity equation and hence it does not even yield convergent solutions. The validity of this assumption was discussed in detail in ref. [5].

The Lewis number, a measure of the relative importance of heat transport to the vapor transport, affects the relative movement of the temperature *wave front* compared to the vapor concentration *wave front*. For the case under investigation with a Lewis number less than one, as it can be seen in Figs. 2 and 3 the

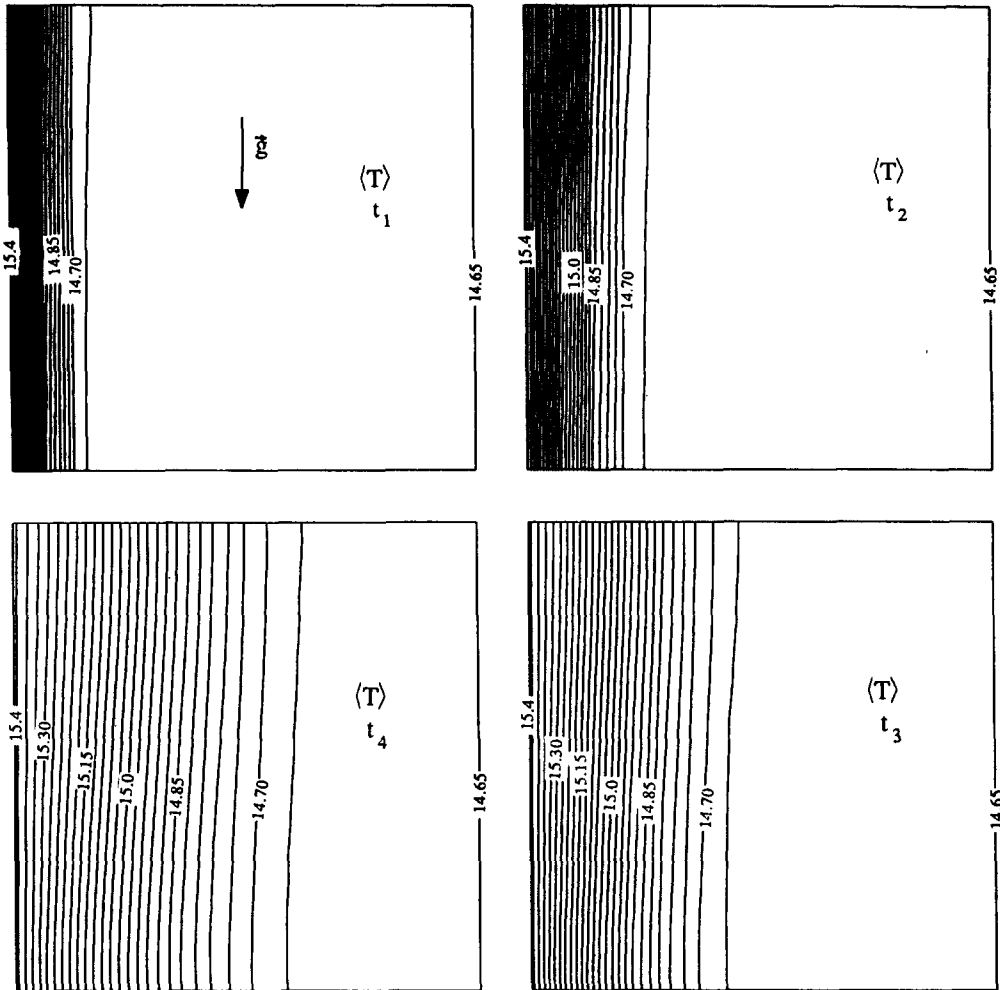


FIG. 2. Spatial variation of temperature inside the porous material for $A = 1$, $\omega_h = 1.0$, at four different times: $t_1 = 0.0005$; $t_2 = 0.0015$; $t_3 = 0.005$; $t_4 = 0.01$.

vapor concentration *wave front* moves faster than the temperature *wave front* as expected. For a Lewis number greater than one, the opposite effect was observed. Another important result which can be observed in Fig. 5 is that the liquid accumulates in the region which is next to the hot and humid environment much more than the rest of the porous matrix.

Figure 6 depicts the velocity field distribution for the gas phase. As it can be seen the flow starts from both the right- and left-hand sides and then moves toward the interior region of the porous insulation since the top and bottom walls are impermeable. Due to the effect of gravity, the fluid moves downward and finally flows out of the porous matrix. This is the only flow configuration that satisfies the gas continuity as well as the gravity requirements. Figure 6 is presented for times t_1 and t_4 only since the velocity distributions at t_2 and t_3 are similar to the velocity distributions at t_1 and t_4 . The contours in Figs. 2, 3 and 5 clearly indicate that the physically pertinent variables are

dependent on both dimensions of the porous matrix especially in the mid-region. Therefore, a one-dimensional analysis would lead to errors especially in the mid-region of the insulation. The two-dimensional behavior results mainly from the fluid motion in the porous matrix. It should be noted that the presented results are for moderate temperature differences imposed across the porous matrix. For larger temperature differences, these two-dimensional distortions will become more pronounced. It should also be noted that higher pressure gradients significantly reduce these two-dimensional distortions. For the sake of brevity, the results for higher pressure gradients are not presented here.

The peculiar signature of the contours, with respect to their curvatures, for the temperature, vapor density and the liquid content can be explained as follows. For the early times such as t_1 , t_2 and t_3 , the *wave fronts* of the contours are essentially in the left half of the spatial domain. Due to the fluid motion, the propa-

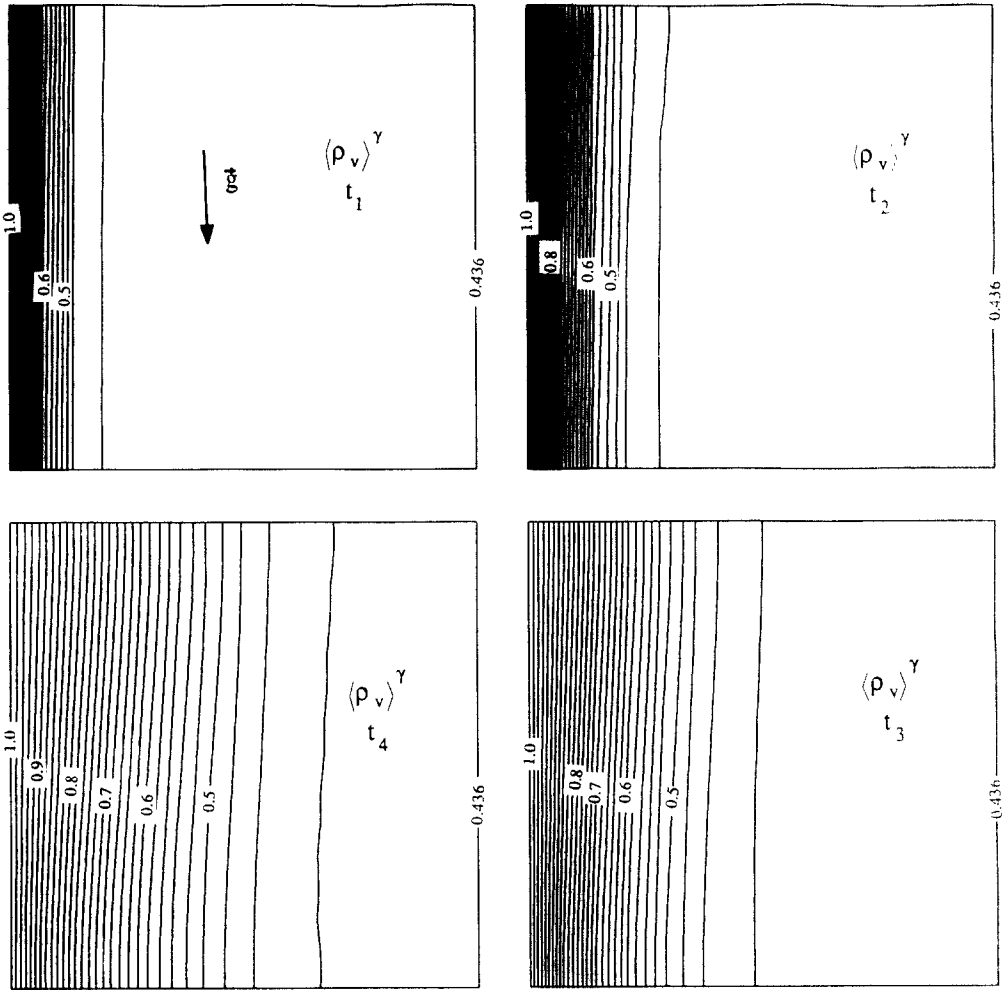


FIG. 3. Vapor density distributions for $A = 1$, $\omega_h = 1.0$, at four different times corresponding to Fig. 2.

gation of the upper half of the *wave fronts* is enhanced whereas the propagation of the lower half of the *wave fronts* is depressed. Therefore, the upper parts of the *wave fronts* are moving faster than the lower parts. Furthermore, the top and bottom walls are impermeable and insulated, making the contours perpendicular to the top and bottom boundaries. The combination of these two effects results in the curvatures which are observed in Figs. 2, 3 and 5. For later times such as t_4 , the *wave fronts* of the contours are in the right half of the porous insulation. The fluid motion hinders the diffusion phenomenon in the upper right region while it assists the diffusion in the lower right region. However, the diffusion in the left domain is still affected by the fluid motion from the left. Therefore, even though the curvilinear shape of the contours experience a gradual change, their overall characteristics are still maintained. It should be noted that the gradual change in the shape of the contours, such as temperature and vapor density contours, might not be so apparent, when the *wave fronts* move

into the right half domain. But at the later times t_5 and t_6 , which will be discussed later on, changes in the signature of these contours become more apparent. As a result of this type of curvature at the same x locations in the insulation, the values of the temperature and vapor density in the upper region are higher than the corresponding values in the lower region. It should also be noted that one might expect that the liquid content values in the lower region should be larger than the values in the upper region as a result of the gravitational force. That this is not so is due to the small amounts of liquid which are formed inside the porous slab, i.e. when $\epsilon_\beta < \epsilon_{\beta p}$ where $\epsilon_{\beta p}$ denotes the liquid content below which the liquid is immobile, the liquid is essentially trapped in the pores. Therefore, the gravity will not have a significant role on ϵ_β and the liquid cannot pile up in the bottom region of the porous material. However, the current solution scheme did account for and incorporated the possibility of the liquid mobility.

Figures 2–6 are based on the case with an aspect

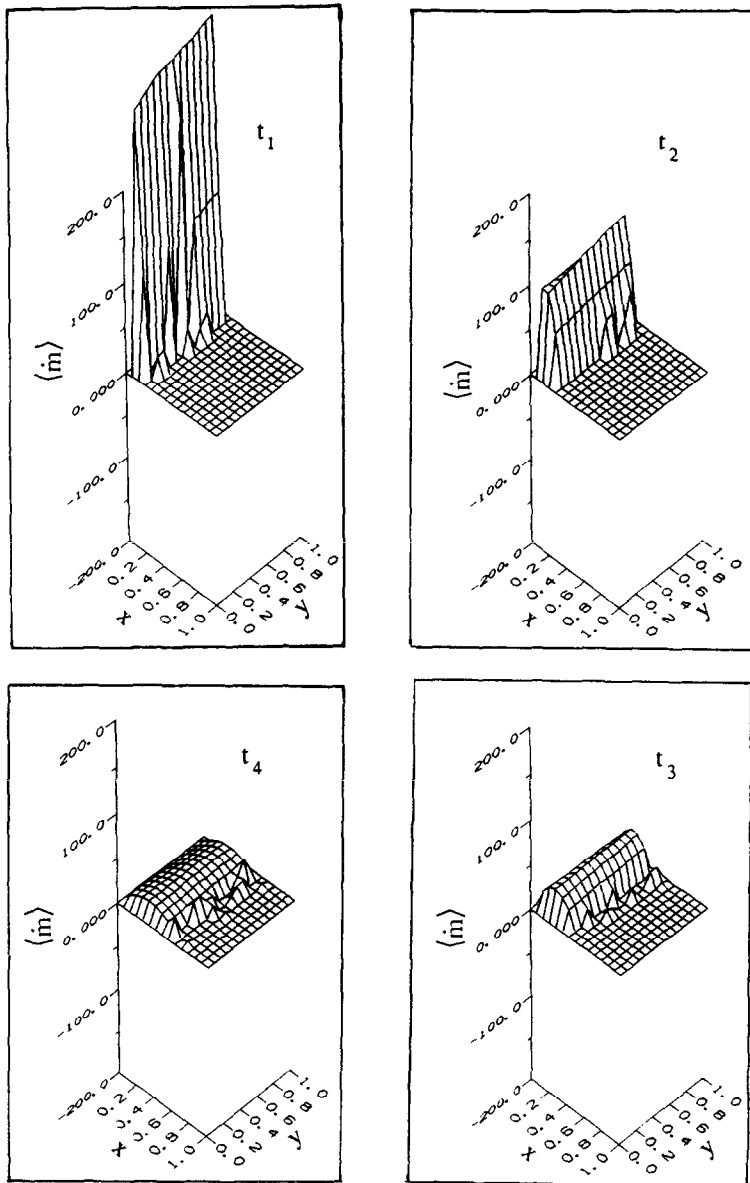


FIG. 4. Three-dimensional condensation rate plots for $A = 1, \omega_h = 1.0$, at four different times corresponding to Fig. 2.

ratio of one and a relative humidity of one at the left boundary. For the case with an aspect ratio of two, the flow field was found to be qualitatively similar to that of an aspect ratio of one. The distributions of the important variables such as the temperature, vapor density, condensation rate, and the liquid content are also qualitatively similar to the case for an aspect ratio of one, and hence they are not presented here. In Fig. 7, the transient non-dimensional heat transfer rates across the hot wall for $A = 1, \omega_h = 1.0$ and $A = 2, \omega_h = 1.0$ are depicted. As it can be seen, there is almost no difference between the two cases. This is due to the similarity between the two configurations, and the identity of the boundary conditions in both cases. A

close examination of Fig. 7 reveals the presence of very small amplitude oscillations, around $t = 0.0014$, in the Nusselt number. This type of oscillating phenomenon was also reported by Patterson and Imberger [18], Penot [19] and Staehle and Hahne [20] in studying transient natural convection flows.

All of the results which were discussed so far were for $\omega_h = 1.0$. To examine the effect of different humidity levels, the results for the vapor density distributions and condensation rate are presented for $\omega_h = 0.8$ and $A = 1$ in Figs. 8 and 9. As expected, the humidity levels at the exterior boundaries have a direct influence on the vapor transport, condensation rate, and hence the liquid content. By comparing Figs.

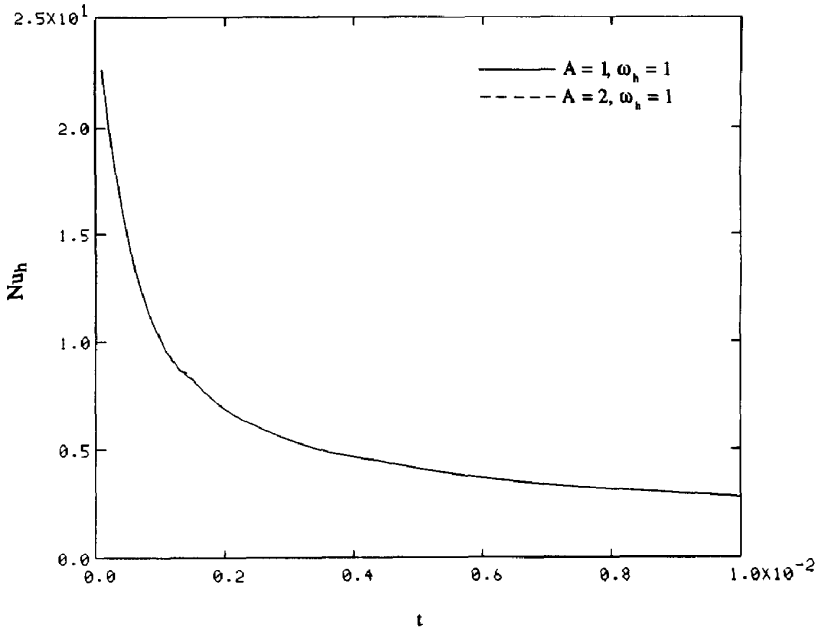


FIG. 7. Effects of the aspect ratio on the transient Nusselt number distribution.

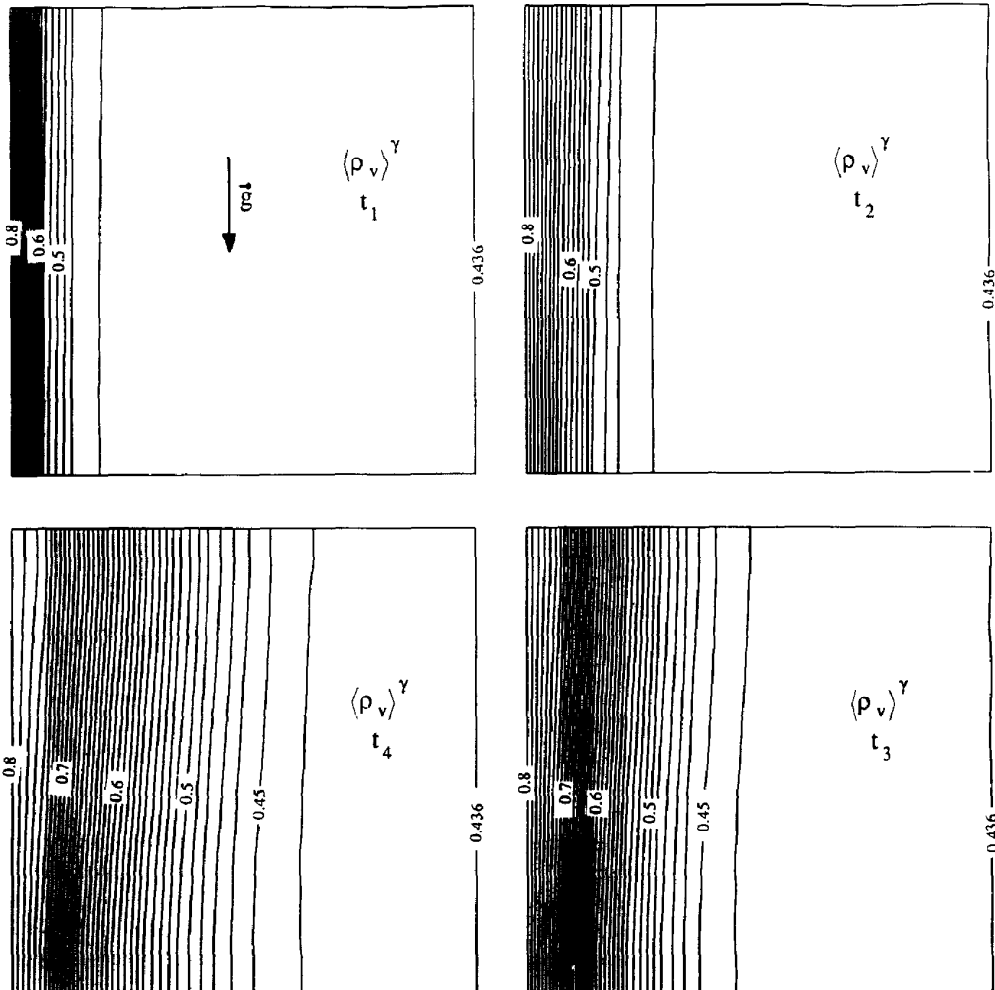


FIG. 8. Vapor density distributions for $A = 1, \omega_h = 0.8$, at four different times corresponding to Fig. 2.

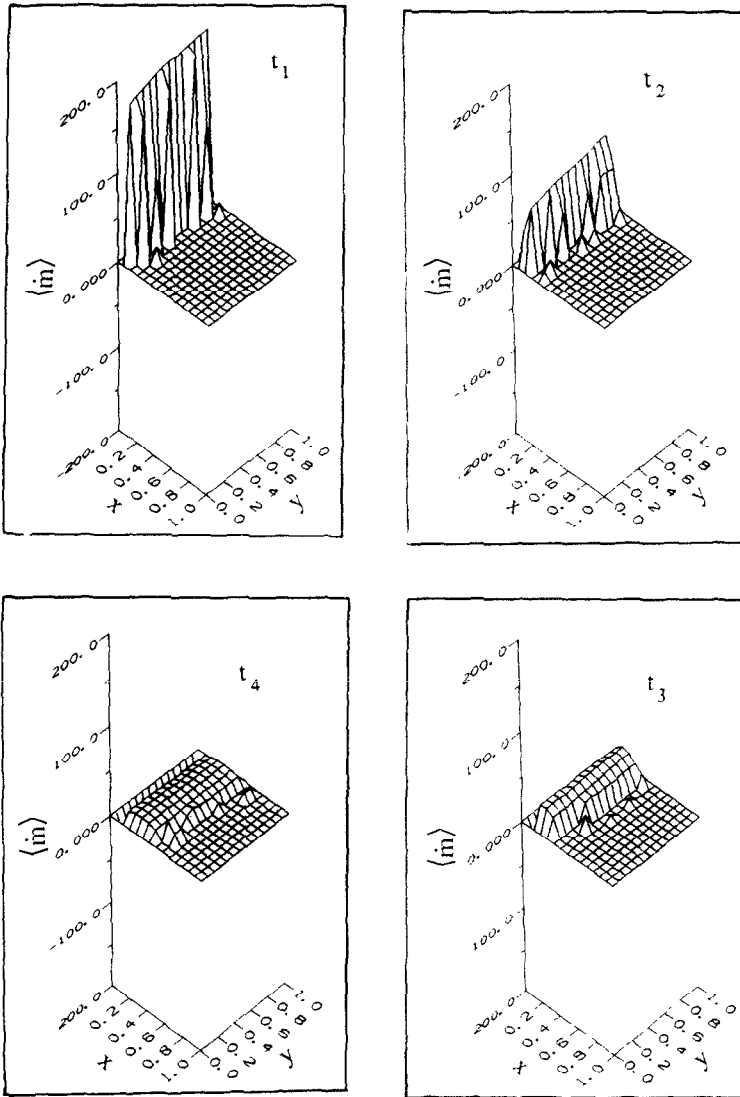


FIG. 9. Three-dimensional condensation and evaporation rate plots for $A = 1$, $\omega_h = 0.8$, at four different times corresponding to Fig. 2.

8 and 9 with Figs. 3 and 4, respectively, it can be found that decreasing the humidity level depresses the vapor transport, the condensation rate and the liquid content. It is also quite interesting to examine the effect of changing the humidity levels on the temperature field while the boundary conditions for the temperature are kept unchanged. If we carefully compare the temperature distributions in Fig. 10 which is for $\omega_h = 0.8$, $A = 1$ with the temperature distributions in Fig. 2 which is for $\omega_h = 1.0$, $A = 1$, we find that the temperature contours are altered due to the change of humidity boundary conditions. For example, the temperature *wave front* for $\omega_h = 1.0$ in Fig. 2 is moving faster than the temperature *wave front* for $\omega_h = 0.8$. This is because increasing the humidity level enhances the vapor transport, and the enhancement in vapor transfer will also cause an increase in energy transfer.

This again indicates another aspect of the complex interaction between the temperature and moisture fields.

Since there were no available analytical or experimental results which could be used for direct comparison, the numerical scheme was benchmarked through various physically pertinent alternatives. First, runs were made for a case dealing with a square porous matrix which is subjected to step-change boundary conditions from all four sides of the matrix. Physically, at the steady state, we would expect that the condensation rate would go to zero everywhere in the matrix and that the variations for all of the field variables would die out and approach the field values at the periphery of the matrix. These expectations were completely verified by our numerical results. It was also found that for this case, the common con-

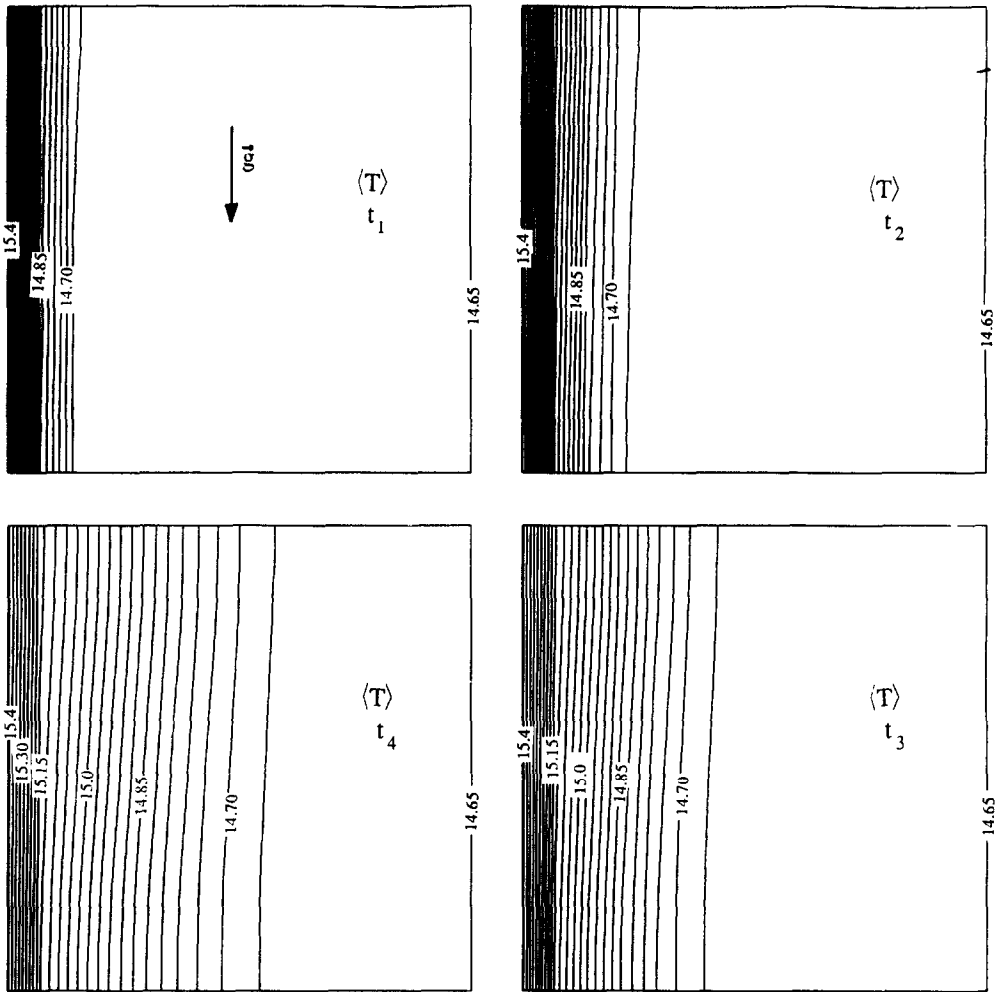


FIG. 10. Temperature distributions for $A = 1$, $\omega_h = 0.8$, at four different times corresponding to Fig. 2.

stant pressure approximation can yield results which are quite close to the ones without such approximation. In fact the constant pressure approximation for this case reduced the CPU time by several orders of magnitude. This was because the magnitude of the gas phase convection terms, which were only gravity driven, in the governing equations was significantly reduced. However, this simplification was found not to be valid for the case under investigation since the gas phase velocity field was totally different from the velocity field which was obtained without employing the constant pressure approximation. Secondly for the limiting case with pure conduction where there is no convection and condensation, it was found that the numerical results agreed very well with the analytical conduction results. Next, the approach toward steady state at longer times was analyzed. Figure 11 shows the temperature and the vapor density contours at later times t_5 and t_6 for the case $A = 1$, $\omega_h = 1$. The approach toward the steady state for the temperature

and vapor density distributions can be clearly observed in these figures. The three-dimensional plots for the condensation rate in Fig. 12 further confirm the above argument as it can be seen that the condensation rate is significantly diminished as time passes by. Furthermore, as mentioned earlier the results for all of the different explicit and semi-implicit schemes which were investigated in this work, were in good agreement with each other.

Finally, the accuracy of the numerical scheme was checked by decreasing the time step size and increasing the number of grids. The results obtained by using different time step sizes while keeping the number of grids constant were found to be in good agreement, both quantitatively and qualitatively. When the number of grids was increased, say from 11×11 to 15×15 and then to 21×21 , the required time step size decreased drastically even though per time step computational time did not increase that much since the computation routine was highly vectorized.

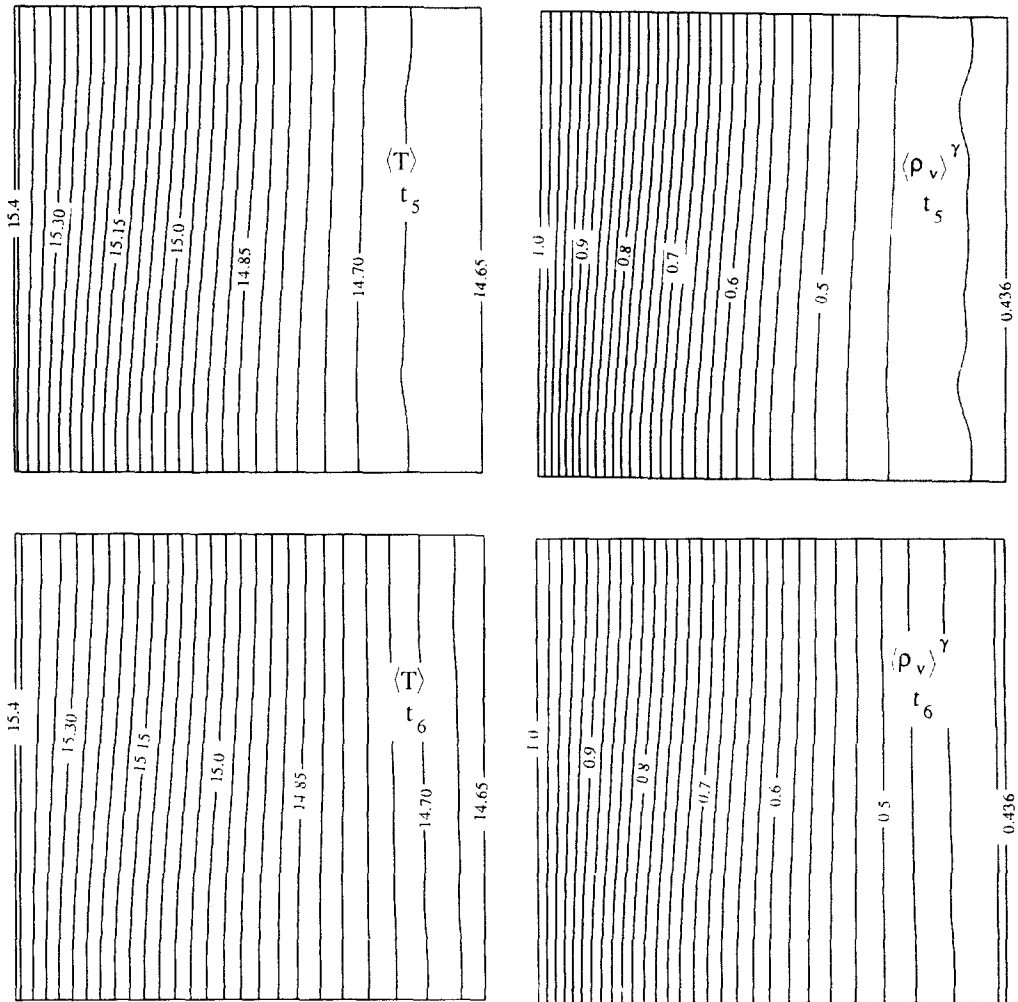


FIG. 11. Temperature and vapor density distributions for $A = 1$, $\omega_h = 1.0$, at later times: $t_5 = 0.02$; $t_6 = 0.03$.

Although the quality of contours was improved by increasing the number of grids, the primary features of contours were not changed. Therefore, most runs were done based on a grid size of 15×15 for $A = 1$ and 15×29 for $A = 2$ except for the results in Figs. 11 and 12, which are based on grids of 11×11 . It should be noted that the numerical computations for these types of problems are extremely intensive. For example after full optimization and strong vectorization of the computation routine, it took about 5.1 h of Cray X-Mp/28 to generate a single curve in Fig. 7. To the authors' knowledge, this type of analysis which fully simulates the multiphase transport process with phase change is presented for the first time.

6. CONCLUSIONS

The phase change process in a porous material was thoroughly analyzed in the present investigation.

The problem which deals with multiphase heat and mass transfer accompanied by phase change in porous media was modelled by a system of transient inter-coupled equations. The problem was analyzed without making any significant simplifications. A final version of an explicit upwind difference scheme which consists of two different formats in time and space accounting for phase change was devised. This scheme was chosen for its better numerical stability compared to the other upwind explicit schemes. The convective terms in the gas phase continuity and diffusion equations were found to be responsible for determining the time step size. Extensive comparisons were made between this scheme and several semi-implicit schemes. It showed that the total CPU time was not reduced by using such semi-implicit schemes. In what follows some of the more significant conclusions are summarized.

- (1) The *wave-like* propagation phenomenon was

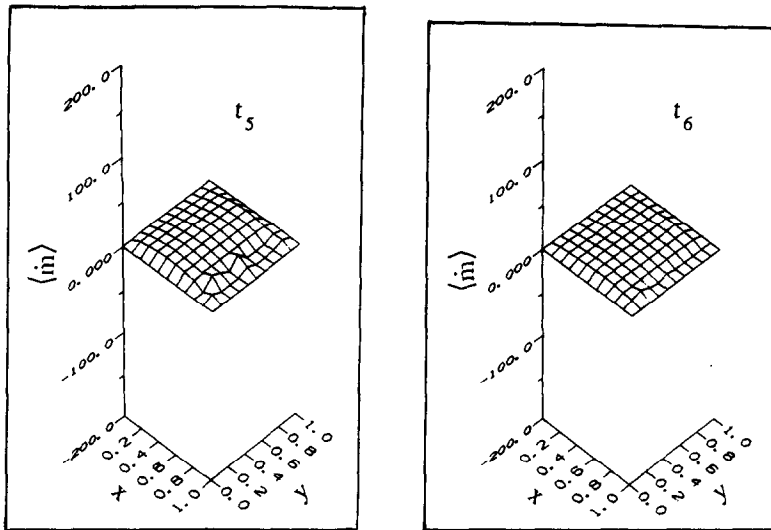


FIG. 12. Three-dimensional condensation rate plots for $A = 1$, $\omega_h = 1.0$, at later times corresponding to Fig. 11.

observed for all of the important field variables such as the temperature, liquid content, vapor density and the condensation rate.

(2) The liquid accumulation was found to be heavily concentrated in the region which was adjacent to the hot and humid environment compared to the remainder of the porous insulation.

(3) The aspect ratio had an insignificant effect on the Nusselt number.

(4) The humidity levels had a direct effect on the vapor transport and condensation process. Increasing the humidity level enhanced the vapor transport, condensation rate, liquid content as well as the energy transfer.

(5) The Lewis number was found to be a very good yardstick for characterizing the relative movement of the temperature *wave front* compared to the vapor density *wave front*. For Lewis numbers less than one, the vapor density *wave front* moves faster than the temperature *wave front*. For Lewis numbers greater than one, the reverse trend was observed.

(6) The one-dimensional model is not valid for a number of situations. This is especially true when the porosity is high and the pressure gradient is very small or zero. However, higher pressure gradients significantly reduce the two-dimensional distortions.

(7) The constant pressure simplification was found to be a good approximation for a case dealing with a porous matrix subjected to step-change boundary conditions on all four sides. Making such a simplification can reduce the CPU time drastically. However, this simplification is not valid for the general case which is considered in this work. This common assumption should be employed with extreme caution for this type of phase change problems.

Acknowledgement—The grant from Ohio Supercomputer Center is acknowledged and appreciated.

REFERENCES

1. R. P. Tye and S. C. Spinney, A study of the effects of the moisture vapor on the thermal transmittance characteristics of cellulose fibre thermal insulation, *J. Thermal Insul.* **2**, 175–196 (1979).
2. M. B. Stewart, An experimental approach to the study of moisture dynamics in walls, *ASTM STP 779*, 92–101 (1982).
3. C. Langlais, M. Hyrien and S. Karlsfeld, Moisture migration in fibrous insulating material under the influence of a thermal gradient, Moisture Migration in Building, *ASTM STP 779*, 191–206 (1982).
4. Y. Ogniewicz and C. L. Tien, Analysis of condensation in porous insulation, *Int. J. Heat Mass Transfer* **24**, 421–429 (1981).
5. K. Vafai and S. Sarkar, Condensation effects in a fibrous insulation slab, *J. Heat Transfer* **108**, 667–675 (1986).
6. K. Vafai and S. Whitaker, Heat and mass transfer accompanied by phase change in porous insulations, *J. Heat Transfer* **108**, 132–140 (1986).
7. S. Whitaker, Simultaneous heat, mass and momentum transfer in porous media: a theory of drying. In *Advances in Heat Transfer*, Vol. 13. Academic Press, New York (1977).
8. P. Vasseur, T. H. Nguyen, L. Robillard and V. K. T. Thi, Natural convection between horizontal concentric cylinders filled with a porous layer with internal heat generation, *Int. J. Heat Mass Transfer* **27**, 337–349 (1984).
9. K. Vafai and C. L. Tien, Boundary and inertia effects on flow and heat transfer in porous media, *Int. J. Heat Mass Transfer* **24**, 195–203 (1981).
10. M. R. J. Wyllie, Relative permeability. In *Petroleum Production Handbook* (Edited by Frick), Vol. 2, Chap. 25. McGraw-Hill, New York (1962).
11. I. Fatt and W. A. Klikoff, Effect of fractional wettability on multiphase flow through porous media. AIME Technical Note No. 2043, *AIME Trans.* **216**, 426–432 (1959).

12. K. S. Udell, Heat transfer in porous media considering phase change and capillarity—the heat pipe effect, *Int. J. Heat Mass Transfer* **28**, 485–495 (1985).
13. M. Kaviany and M. Mittal, Funicular state in drying of a porous slab, *Int. J. Heat Mass Transfer* **30**, 1407–1418 (1987).
14. S. Whitaker, Toward a diffusion theory of drying, *Ind. Engng Chem. Fundam.* **16**, 408–414 (1977).
15. S. Whitaker and W. T.-H. Chou, Drying granular porous media—theory and experiment, *Drying Technol.* **1**, 3–33 (1983).
16. D. A. Anderson, J. C. Tannehill and R. H. Pletcher, *Computational Fluid Mechanics and Heat Transfer*. McGraw-Hill, New York (1984).
17. G. B. Reddy, J. C. Mulligan and R. R. Johnson, Analysis of heat and mass transfer in unsaturated porous materials: an application to soil with a heat source. In *Multiphase Transport in Porous Media*, Vol. 60, pp. 77–84. ASMEFED (1987).
18. J. Patterson and J. Imberger, Unsteady natural convection in a rectangular cavity, *J. Fluid Mech.* **100**, 65–86 (1980).
19. F. Penot, Numerical calculation of two-dimensional natural convection in isothermal open cavities, *Numer. Heat Transfer* **5**, 421–437 (1982).
20. B. Staehle and E. Hahne, Overshooting and damped oscillations of transient natural, convection flows in a cavity, *Proc. Seventh Int. Heat Transfer Conf.*, Vol. 2, pp. 287–292 (1982).

APPENDIX

The dimensionless variables are defined as

$$x = \frac{\bar{x}}{\bar{L}}, \quad y = \frac{\bar{y}}{\bar{L}}, \quad t = \frac{\bar{\alpha}_{\text{eff},0} \bar{t}}{\bar{L}^2} \quad (\text{A1})$$

$$\mathbf{v}_\beta = \frac{\bar{\mathbf{v}}_\beta \bar{L}}{\bar{K} \bar{K}_c / \bar{\mu}_\beta}, \quad \mathbf{v}_\gamma = \frac{\bar{\mathbf{v}}_\gamma}{\bar{\tau}_{\gamma,0}} \quad (\text{A2})$$

$$T = \frac{\bar{T}}{\Delta \bar{T}}, \quad \dot{m} = \frac{\bar{m} \bar{L}^2 \Delta \bar{h}_{\text{vap}}}{\bar{K}_{\text{eff},0} \Delta \bar{T}} \quad (\text{A3})$$

$$\rho_l = \frac{\bar{\rho}_l}{\bar{\rho}_{\gamma,0}}, \quad p_l = \frac{\bar{p}_l}{\bar{p}_{\gamma,0}}, \quad \mathbf{g} = \frac{\bar{\mathbf{g}}}{\bar{g}_0} \quad (\text{A4})$$

and the dimensionless parameters are defined as

$$P_1 = \frac{\bar{\rho}_\beta}{\bar{\rho}_0}, \quad P_2 = \frac{\bar{c}_\beta}{\bar{c}_0}, \quad P_3 = \frac{\langle \bar{c}_\gamma \rangle}{\bar{c}_0} \quad (\text{A5})$$

$$P_4 = \frac{\bar{\rho}_{\gamma,0}}{\bar{\rho}_0}, \quad P_5 = \frac{\bar{\rho}_{\gamma,0} \bar{g}_0 \bar{L}}{\bar{p}_{\gamma,0}}, \quad P_6 = \frac{\Delta \bar{h}_{\text{vap}}}{\bar{c}_0 \Delta \bar{T}} \quad (\text{A6})$$

$$P_9 = \frac{\Delta \bar{T}}{\bar{T}_0}, \quad P_{11} = \frac{\bar{\rho}_{\gamma,0}}{\bar{\rho}_{\gamma,0}}, \quad P_{12} = \frac{\bar{\rho}_{a,0}}{\bar{\rho}_{\gamma,0}} \quad (\text{A7})$$

$$P_{13} = \frac{\bar{p}_{\gamma,0}}{\bar{p}_{\gamma,0}}, \quad P_{14} = \frac{\bar{p}_{a,0}}{\bar{p}_{\gamma,0}}, \quad P_{15} = \frac{2\bar{\sigma}_{\beta\gamma}}{r \bar{\rho}_\beta \bar{R}_v \Delta \bar{T}} \quad (\text{A8})$$

$$P_{16} = \frac{\Delta \bar{h}_{\text{vap}}}{\bar{R}_v \Delta \bar{T}}, \quad P_{18} = \frac{\bar{\alpha}_{\text{eff}}}{\bar{\alpha}_{\text{eff},0}}, \quad P_{19} = \frac{\bar{K}_{\text{eff}}}{\bar{K}_{\text{eff},0}} \quad (\text{A9})$$

$$P_{20} = \frac{\bar{K} \bar{\rho}_{\gamma,0}}{\bar{\mu}_\gamma \bar{L} \bar{v}_{\gamma,0}}, \quad P_e = \frac{\bar{v}_{\gamma,0} \bar{L}}{\bar{\alpha}_{\text{eff},0}}, \quad Le = \frac{\bar{\alpha}_{\text{eff},0}}{\bar{D}_{v,\text{eff}}} \quad (\text{A10})$$

$$\psi_\tau = \frac{\bar{K}_c \bar{\tau}_\gamma \Delta \bar{T}}{\bar{K}_c}, \quad \psi_g = \frac{(\bar{\rho}_\beta - \bar{\rho}_\gamma) \bar{g}_0 \bar{L}}{\bar{K}_c}, \quad \psi_\iota = \frac{\bar{K} \bar{K}_c}{\bar{\mu}_\beta \bar{\alpha}_{\text{eff},0}} \quad (\text{A11})$$

ETUDE NUMERIQUE DES EFFETS DE CHANGEMENT DE PHASE DANS LES MATERIAUX POREUX

Résumé—On développe une étude numérique du transfert de chaleur et de masse avec changement de phase dans des matériaux poreux. Le problème est modélisé par un système d'équations couplées qui représente le mécanisme de transport bidimensionnel et multiphasique dans les milieux poreux. La solution est une simulation complète sans aucune simplification. On dégage et discute en détail les variations et les interdépendances entre la température, la densité de vapeur, le taux de condensation, la fraction liquide et les champs de vitesse du fluide. On trouve que l'accroissement du facteur de forme de la matrice poreuse diminue sensiblement le nombre de Nusselt et que l'augmentation du niveau d'humidité accroît la condensation, le transport de vapeur et le transfert d'énergie. On trouve que le modèle monodimensionnel n'est pas valable quand les frontières de la matrice poreuse sont soumises à une différence de pression faible ou nulle et que la simplification d'une pression uniforme conduit à des erreurs sensibles dans certaines circonstances. L'analyse, qui présente une simulation complète pour la première fois, peut être appliquée à une classe de problèmes de transport de chaleur et de masse avec changement de phase à travers un milieu poreux.

NUMERISCHE UNTERSUCHUNG DER PHASENÄNDERUNG IN PORÖSEN MATERIALIEN

Zusammenfassung—Diese numerische Untersuchung behandelt die Wärme- und Stoffübertragung mit Phasenwechsel in porösen Materialien. Dies wird durch ein System von gekoppelten, instationären Differentialgleichungen modelliert und umfaßt eine zweidimensionale Betrachtung der mehrphasigen Transportvorgänge. Der Algorithmus erlaubt eine vollständige Simulation ohne wesentliche Vereinfachungen. Die Zusammenhänge zwischen Temperatur, Dampfdichte, Kondensationsrate, Flüssigkeitsanteil und Geschwindigkeitsfeld werden ausführlich diskutiert und demonstriert. Eine Vergrößerung des Seitenverhältnisses der porösen Matrix senkt die Nusseltzahl erheblich, eine Erhöhung der Feuchtigkeit verbessert die Kondensation, den Dampftransport und die Energieübertragung. Außerdem hat sich gezeigt, daß ein eindimensionales Modell dann nicht verwendet werden darf, wenn die Druckdifferenz am Rand der Matrix klein ist, und daß die Annahme eines konstanten Drucks unter Umständen sehr große Fehler mit sich bringt. Die Analyse ermöglicht zum ersten Mal eine vollständige Simulation und kann auf viele Phasenwechselprobleme in porösen Medien angewandt werden.

ЧИСЛЕННОЕ ИССЛЕДОВАНИЕ ЭФФЕКТОВ ФАЗОВОГО ПЕРЕХОДА В ПОРИСТЫХ МАТЕРИАЛАХ

Аннотация—Численно исследован тепло- и массоперенос с фазовым переходом в пористых материалах. Двумерный многофазный перенос моделируется системой взаимосвязанных уравнений. Алгоритм нахождения решения позволяет проводить моделирование без существенных упрощений. Подробно обсуждается взаимосвязь между полями температуры, плотности пара, скорости конденсации, содержания жидкости и ее скорости. Обнаружено, что при увеличении отношения сторон пористой матрицы значительно уменьшается число Нуссельта, а при возрастании влажности усиливаются конденсация, перенос пара и энергии. Также установлено, что одномерная модель неприменима, когда на границе пористой матрицы перепад давления мал или равен нулю, а предположение постоянства давления для некоторых случаев может привести к значительным погрешностям. Данный анализ может применяться к целому классу задач тепло- и массопереноса с фазовым переходом в пористой среде.